Title

S = 3 Ground State for a Tetranuclear MnIV 4O4 Complex Mimicking the S3 State of the Oxygen-Evolving Complex

Journal

Journal of the American Chemical Society, 142(8)

ISSN

0002-7863

Authors

Lee, Heui Beom
Marchiori, David A
Chatterjee, Ruchira
et al.

Publication Date

2020-02-26

DOI

10.1021/jacs.9b10371

Peer reviewed

HHS Public Access

Author manuscript

J Am Chem Soc. Author manuscript; available in PMC 2020 May 19.

Published in final edited form as:

J Am Chem Soc. 2020 February 26; 142(8): 3753–3761. doi:10.1021/jacs.9b10371.

S = 3 Ground State for a Tetranuclear $Mn^{IV}_4O_4$ Complex Mimicking the S_3 state of the Oxygen Evolving Complex

Heui Beom Lee[†,§], **David A. Marchiori**[‡,§], **Ruchira Chatterjee**[‖], **Paul H. Oyala**[†], **Junko Yano**[‖], **R. David Britt**[*,‡], **Theodor Agapie**[*,†]

[†]Department of Chemistry and Chemical Engineering, California Institute of Technology, 1200 E California Blvd MC 127-72, Pasadena, California 91125, United States

[‡]Department of Chemistry, University of California Davis, One Shields Avenue, Davis, California 95616, United States

[‖]Molecular Biophysics and Integrated Bioimaging Division, Lawrence Berkeley National Laboratory, Berkeley, CA 94720, United States

Abstract

The S_3 state is currently the last observable intermediate prior to O–O bond formation at the oxygen evolving complex (OEC) of Photosystem II, and its electronic structure has been assigned to a homovalent Mn^{IV}_4 core with an $S = 3$ ground state. While structural interpretations based on the EPR spectroscopic features of the S_3 state provide valuable mechanistic insight, corresponding synthetic and spectroscopic studies on tetranuclear complexes mirroring the Mn oxidation states of the S_3 state remain rare. Herein, we report the synthesis and characterization by XAS and multifrequency EPR spectroscopy of a $Mn^{IV}_4O_4$ cuboidal complex as a spectroscopic model of the S_3 state. Results show that this $Mn^{IV}_4O_4$ complex has an $S = 3$ ground state with isotropic ^{55}Mn hyperfine coupling constants of −75, −88, −91, and 66 MHz. These parameters are consistent with an αααβ spin topology approaching the trimer-monomer magnetic coupling model of pseudo-octahedral Mn^{IV} centers. Importantly, the spin ground state changes from $S = 1/2$ to $S = 3$ as the OEC is oxidized from the S_2 state to the S_3 state. This same spin state change is observed following the oxidation of the previously reported $Mn^{III}Mn^{IV}_3O_4$ cuboidal complex to the $Mn^{IV}_4O_4$ complex described here. This sets a synthetic precedent for the observed low-spin to high-spin conversion in the OEC.

Geaphical Abstract

[*]**Corresponding Author:** agapie@caltech.edu, rdbritt@ucdavis.edu.
[§]Authors contributed equally to this work

Supporting Information. Experimental procedures and characterization. This material is available free of charge via the Internet at http://pubs.acs.org.

The authors declare no competing financial interest.

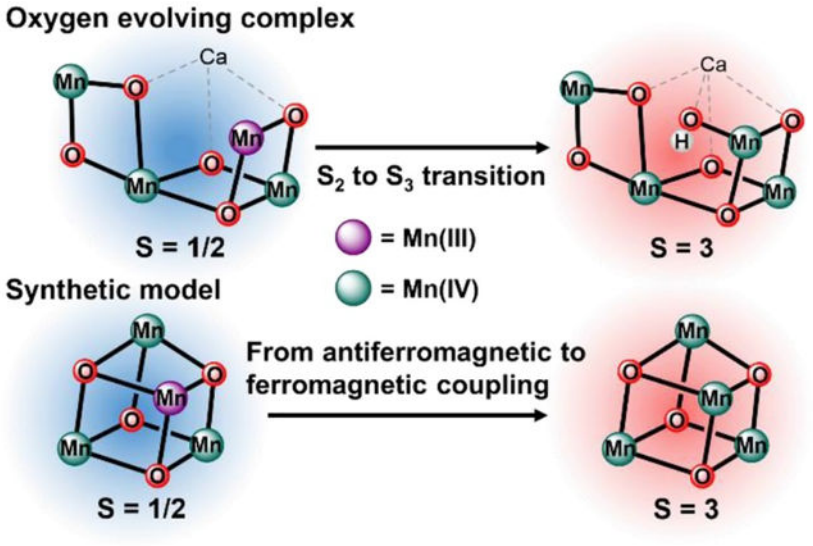

INTRODUCTION

Mechanistic studies of biological water oxidation at the oxygen evolving complex (OEC) of Photosystem II (PSII) are performed in the context of the Kok cycle of S_n (n = 0−4) states.[1–4] Starting from the dark stable S_1 state, sequential light-induced one electron oxidations lead to the progression to higher S_n states, resulting in the formation of the S_3 state, the last observable intermediate prior to dioxygen formation.[5–6] Involving a series of elementary steps that include H^+ transfer, substrate H_2O binding, and e^- transfer, the $S_2 \rightarrow S_3$ transition represents a critical, sensitive step in the catalytic cycle of the OEC, as discrete changes to the OEC precede the formation of the S_3 state.[7–8] Despite being the subject of extensive biochemical, structural, spectroscopic, and computational studies, the (electronic) structure and the mechanism of formation of the S_3 state remain largely unknown.[7–23] To obtain a better understanding of the properties of the S_3 state, systematic structure-function (property) studies on relevant model complexes are necessary. Despite significant efforts to prepare tetra- and pentanuclear complexes as models of the OEC, relevant complexes in terms of structure, redox state, spectroscopy, and reactivity are rare.[24–38]

On the basis of EPR, MCD, and X-ray spectroscopic studies, the electronic structure of the S_3 state has been assigned to a homovalent Mn^{IV}_4 core with an $S = 3$ spin ground state.[5, 39–41] Two structural isomers S_3^A (dimer-of-dimers) and S_3^B (trimer-monomer), both with $S = 3$ spin ground states, have been invoked for the S_3 state (Figure 1a).[5, 42] A similar structural isomerism has been proposed for the S_2 state.[24, 43] Such proposed structural changes may lead to differences in the sign and magnitude of the magnetic exchange interactions (J_{ij}) between adjacent Mn centers, which in turn affect not only the spin ground state of the cluster but also the observed sign and magnitude of the projected ^{55}Mn hyperfine interactions (A_i).[43–44] The observed A_i for Mn ions in the S_3 state have been accommodated with the calculated J_{ij} for the S_3^A structure.[5] The high-resolution (2.04 Å) structure of the S_3 state obtained at room temperature using femtosecond X-ray free electron laser (XFEL) techniques is similar to the S_3^A structure.[10] Further improvements in resolution and different

sample conditions need to be addressed to identify possible contributions from structural isomers such as the proposed S_3^B state.[10, 45]

Comparative studies on structurally related $Mn^{III}Mn_3^{IV}$ and Mn^{IV}_4 complexes as models of the S_2 and S_3 states may prove beneficial, but due to synthetic difficulties, such studies have been reported for only two classes of tetranuclear Mn complexes: linear and adamantane-shaped complexes, both featuring $[Mn_4O_6]^{n+}$ cores (Figure 1b).[46–52] For the linear $[Mn^{IV}_4O_6(bpy)_6]^{4+}$ complex, strong pairwise antiferromagnetic interactions lead to a diamagnetic $S = 0$ ground state;[46, 51] reduction to the $[Mn^{III}Mn^{IV}_3O_6(bpy)_6]^{3+}$ complex by radiolysis leads to an $S = 1/2$ ground state, featuring the characteristic multiline EPR signal at $g = 2$.[53] For the adamantane-shaped $[Mn^{IV}_4O_6(tacn)_4]^{4+}$ complex and related ligand substitution series, magnetic susceptibility studies indicate overall ferromagnetic interactions giving rise to an $S = 6$ ground state.[47] EPR studies for the adamantane-shaped complexes have not been reported. An $S = 5/2$ ground state has been reported for a reduced adamantane-shaped complex featuring a $[Mn^{III}Mn^{IV}_3O_6]^{3+}$ core.[54] While both reduced linear ($S = 1/2$) and adamantane-shaped ($S = 5/2$) $Mn^{III}Mn^{IV}_3$ complexes serve as spectroscopic models of the S_2 state, with two possible spin ground states $S = 1/2$ and $S = 5/2$, a Mn^{IV}_4 complex with an $S = 3$ ground state mimicking the S_3 state has not been reported.

Herein, we report the synthesis and characterization by XAS and multifrequency EPR spectroscopies of a unique $Mn^{IV}_4O_4$ cuboidal complex as a spectroscopic model of the S_3 state. Results show that the $Mn^{IV}_4O_4$ complex has an $S = 3$ ground state with isotropic ^{55}Mn hyperfine coupling constants −75, −88, −91, and 66 MHz. These parameters are consistent with an $\alpha\alpha\alpha\beta$ spin topology approaching the trimer-monomer magnetic coupling model of pseudo-octahedral Mn^{IV} centers. Importantly, the spin state change from $S = 1/2$ to $S = 3$, characteristic of the $S_2 \rightarrow S_3$ transition in the OEC, is the same spin state change observed in the oxidation of the previously reported $Mn^{III}Mn_3^{IV}O_4$ cuboidal complex to the $Mn^{IV}_4O_4$ complex, providing the first synthetic precedent for the observed low-spin to high-spin transition in the OEC.

RESULTS

Synthesis.

The diamidate-bridged cuboidal complex $LMn^{III}_2Mn^{IV}_2O_4(diam)(OAc)$ (**1**) was used as a precursor for the targeted $Mn^{IV}_4O_4$ complex (Scheme 1).[24] In propylene carbonate, the cyclic voltammogram of **1** shows a reversible oxidation to the previously characterized one electron oxidized $Mn^{III}Mn_3^{IV}O_4$ complex (**2**) at −50 mV vs Fc/Fc^+.[24] A second quasi-reversible $Mn^{III}Mn_3^{IV}/Mn^{IV}_4$ couple is observed at +780 mV vs Fc/Fc^+ (Figure S3). Notably, formation of the Mn^{IV}_4 species is not observed for analogous tris-acetate or tris-phosphinate complexes, highlighting the ability of amidate ligands in supporting high oxidation state complexes.[55] Accordingly, treatment of **1** with an optimal amount of tris(2,4-dibromophenyl)aminium hexachloroantimonate ($E_{1/2}$ = +1140 mV vs Fc/Fc^+ in MeCN)[56–57] in thawing MeCN leads to the formation of the two electron oxidized $Mn^{IV}_4O_4$ complex (**3**). Addition of fewer equivalents of the aminium oxidant leads to a mixture of **2** and **3** by ^1H NMR (Figure S1), suggesting that **3** is related to **2** by a one electron oxidation. While the

ESI-MS of **2** shows only one peak at m/z = 1354 consistent with the mass of $[LMn_4O_4(diam)(OAc)]^+$, the ESI-MS of **3** shows an additional, major peak at m/z = 677 consistent with the mass of $[LMn_4O_4(diam)(OAc)]^{2+}$ (Figure S2), supporting the $[LMn^{IV}_4O_4(diam)(OAc)][SbCl_6]_2$ formulation of **3**. Overall, complexes **1**, **2**, and **3** represent a rare redox series of essentially isostructural compounds in which the Mn oxidations states of each compound mirror those in the S_1, S_2, and S_3 states, respectively.

X-ray spectroscopy.

Frozen solution Mn K-edge X-ray absorption near-edge spectroscopy (XANES) and extended X-ray absorption fine structure (EXAFS) were used to further characterize metal oxidation states and to provide evidence of structural similarity between **2** and **3** in solution (Figure 2). Absorption edge energies were determined from the second-derivative zero-crossings, giving the following values (eV): 6552.4 (**2**) and 6553.2 (**3**). The positive shift in the edge energy by 0.8 eV is consistent with a Mn centered oxidation, supporting the Mn^{IV}_4 assignment for **3**. In comparison, the edge energy of the S_2 and S_3 states of cyanobacteria PSII are 6554.1 and 6554.4 eV, respectively.[58] The smaller edge energy shift in the $S_2 \rightarrow S_3$ transition in PSII could be due to changes in Mn coordination sphere, such as binding of substrate water.[10] The k^3-weighted EXAFS spectra of **2** and **3** are nearly superimposable (Figure 2b, see SI for fit). A similar set of parameters (Table S1) were used to fit the EXAFS spectra of **2** and **3**, and results show that within error, average Mn-ligand and Mn-Mn distances are similar between **2** and **3**. While small geometrical changes in **3** are not resolved by EXAFS, such as the contraction of a specific Mn-oxo distance (by *c.a.* 0.2 Å) upon oxidation from $Mn^{III}_2Mn^{IV}_2$ (**1**) to $Mn^{III}Mn^{IV}_3$ (**2**), indicative of the Jahn-Teller-like effect in pseudo-octahedral Mn^{III} centers, the X-ray spectroscopic data support the structural integrity of **3** as a cuboidal $Mn^{IV}_4O_4$ cluster.

EPR spectroscopy.

To obtain a better understanding of the spin ground state and the nature of the magnetic coupling interactions between Mn centers, D-band (130 GHz) EPR studies were conducted on frozen solution samples of **3** (Figure 3). Spanning approximately 4 T, the spectrum features five resolved lines (inflection points; see Figure S6 for pseudomodulated spectrum) at 3.4, 4, 5.2, 6, and 6.9 T, with the central feature at 4.63 T (g = 2.01) overlapping with a Mn^{II} impurity *vide infra*. On the basis of the rising edge energy of the XANES spectrum for complex **3** (Figure 2a), the average Mn oxidation state in the sample is increasing, with a small Mn^{II} impurity contributing to the EPR signal at the temperatures studied. EDNMR at the central 4.63 T feature (Figure S8) resolves NMR transitions at approximately 302, 417, and 544 MHz, characteristic of Mn^{II} (S = 5/2) with A_{iso} = 240 MHz. The Mn^{II} feature is simulated with ZFS parameters D and E/D of 0.06 cm^{-1} and 0.167 respectively, in line with reported spin Hamiltonian parameters of Mn^{II}.[59–60] Excluding this central feature, the large spectral breadth of the EPR envelope is indicative of a complex with a large zero-field splitting (ZFS) parameter, while the distribution of the EPR spectrum is suggestive of a positive ZFS parameter and small rhombicity.

Electron spin nutation experiments can be used to assign the spin ground state of EPR active compounds.[5, 61] A variable microwave preparation pulse is applied and followed by a Hahn

echo sequence. This preparation pulse nutates the electron spin, causing the magnitude of the observed spin echo to oscillate. The period of this oscillation is inversely proportional to the magnitude of the effective spin. Electron spin nutation experiments on the high-field edge of the EPR envelope (7 T) were performed to assign the spin state of **3** (inset of Figure 3). An $S = 1/2$ spin standard is needed to assign the spin state of the measured EPR transition: α,γ-bisdiphenylene-β-phenylallyl (BDPA), an $S = 1/2$ radical, was used to this effect. The nutation period of **3** is shorter than that of BDPA by approximately a factor of 2.8. This value is in good agreement with the expected factor of $\sqrt{6} \approx 2.45$ for the $|-3\rangle \rightarrow |-2\rangle$ transition in an $S = 3$ spin system.[5] The slight discrepancy likely arises because the external spin standard BDPA is measured separately from **3**. The conversion factor, the difference between the incident power and the power at the sample, cannot be assumed to be identical from sample to sample as is the case of the internal Y_D radical species present in PSII samples poised in the S_3 state.[5] Despite the slight discrepancy in the expected nutation period for **3**, an intense feature at $g = 12$ in the parallel mode X-band EPR spectrum of **3** (Figure 4) supports the $S = 3$ spin state assignment. The $g = 12$ signal is reminiscent of the spectrum observed for the S_3 state of *T. Elongatus* PSII and other $S = 3$ systems.[5–6, 62]

Spin Hamiltonian simulations of **3** were performed using an $S = 3$ spin state and an isotropic g-value of $g = 1.97$. In higher spin systems ($S > 1/2$), the breadth of EPR spectra depends largely on the axial ZFS parameter D, which removes the degeneracy of the $|\pm m_s\rangle$ states; following the electron Zeeman effect, the magnitude of D determines the magnetic field position of a given EPR transition (Figure S5). Based on the breadth of the EPR envelope, the ZFS parameter in **3** was estimated to be $D = +0.4$ cm^{-1}. The spacing of the turning points (individual m_S levels) is dictated by the ratio of E/D, where E represents the rhombicity of the ZFS. Based on the observed distribution, E/D was estimated to be 0.1. The observed ZFS in **3** is larger than that of the S_3 state of *T. Elongatus* and chemically modified *T. Elongatus* PSII ($|D| = 0.175$ and 0.281 cm^{-1}, respectively)[5, 63] and that of the biomimetic $CaMn_3^{IV}O_4$ model ($|D| = 0.068$ cm^{-1})[36]. Monomeric octahedral Mn^{IV} compounds are useful benchmarks for interpreting spin Hamiltonian parameters of more complex systems such as the S_3 state.[5] Typical ZFS values for monomeric octahedral Mn^{IV} compounds are relatively small, on the order of 0.2 cm^{-1}, due to the near spherical symmetry of the ($t_{2g}^3 e_g^0$) electronic configuration,[64–65] but values in the range of $|D| = 0.17$~2.3 cm^{-1} have been reported for six-coordinate mononuclear Mn^{IV} complexes.[66–68]

EDNMR spectroscopy.

To gain a better understanding of the ^{55}Mn hyperfine interactions in **3**, electron-electron double resonance detected NMR (EDNMR) spectra were collected at selected field positions within the D-band EPR spectrum (Figure 5). EDNMR utilizes a high-turning angle (HTA) pulse to excite formally forbidden transitions ($\Delta m_S = \pm 1$, $\Delta m_I = \pm 1, \pm 2$, etc.), which can be then detected via a Hahn echo sequence.[69–70] The HTA pulse is of a different excitation frequency than pulses in the Hahn echo sequence. When the difference in these frequencies corresponds to a nuclear transition frequency, a decrease in the Hahn echo is observed, which is interpreted as a peak in Figure 5. As with electron nuclear double resonance (ENDOR), EDNMR allows for the detection of nuclear transitions and has been shown to be an important spectroscopic tool at high microwave frequencies.[71] The field dependent

EDNMR spectra of **3** display a number of transitions ranging from 10 to 320 MHz (Figure 5). These features arise from the hyperfine coupling interaction A of the ^{55}Mn nuclei (I = 5/2) and the S = 3 electron spin of complex **3**. The positions of these transitions are dictated by A and the Larmor frequency (ν_n) of the ^{55}Mn nuclei. Depending on the specific $|m_s\rangle$ level being pumped, features in the field-dependent EDNMR are observed at multiples of $|A| \pm \nu_n$ (see SI). Spin Hamiltonian simulations of the ^{55}Mn EDNMR are shown in the colored traces in Figure 5, and the corresponding A values are listed in Table 1. One positive and three negative A values are needed to accurately simulate the EDNMR spectra. This is evidenced by the field-dependent shift of the peaks at 200 (Mn2, blue peaks, Figure 5) and 150 MHz at 7 T (Mn4, cyan peaks, Figure 5) to higher frequencies with decreasing magnetic field, indicating that both Mn2 and Mn4 have negative A values. The shift of the peak at 250 MHz (Mn1, yellow peaks, Figure 5) at 7 T to lower frequencies with decreasing magnetic field indicates that Mn1 has a positive A value. To obtain $|A|$, for example, the yellow peak at 270 MHz at 7 T corresponds to $|A|$ = 65 MHz according to the formula $n|A| + \nu_n$, where n is 3 for the $m_S = |-3\rangle$ to $|-2\rangle$ manifold and ν_n is 74 MHz ($\nu_n(^{55}\text{Mn})$ varies linearly with magnetic field as 10.554 MHz/T).

Typical Mn^{IV} ions in octahedral coordination environments exhibit little ^{55}Mn hyperfine anisotropy by virtue of the spherical symmetry of the half-filled t_{2g} set of d-orbitals, and thus produce sharp ^{55}Mn NMR lines.[5] The EDNMR of **3** is complicated by multiple overlapping transitions, but at fields greater than 5 T, distinct, sharp transitions are observable, characteristic of an all-octahedral Mn^{IV}_4 complex. Due to the relative breadth of the EDNMR peaks (*e.g.* FWHM = 34 MHz for the feature centered at 197 MHz in the EDNMR trace recorded at 7 T) it is difficult to precisely determine the hyperfine anisotropy of all the individual Mn^{IV} ions. However, inspection of transitions at 150 MHz and 270 MHz in the EDNMR trace recorded at 7 T suggests that the hyperfine anisotropy for Mn1 and Mn4 is on the order of 10 MHz. This hyperfine anisotropy is in line with reported values of monomeric octahedral Mn^{IV} as well as the S_3 state.[5] The site-specific anisotropy can be calculated from the projection factors listed in Table 1 and yield values of approximately 25 MHz, which are in good agreement with rhombically distorted octahedral Mn^{IV} in SnO_2/TiO_2.[64,72–73] Mn^{IV} in SnO_2/TiO_2 similarly displays ZFS values on the order of a wavenumber[64, 72–73] suggesting that a distortion of the octahedral coordination environment of the individual Mn^{IV} ions in **3** leads to the observed ZFS.

In exchange-coupled systems, the observed sign and magnitude of the hyperfine coupling interactions reflect the nature of the magnetic exchange interactions between the metal centers. For **3**, a trimer-monomer magnetic coupling model of pseudo-octahedral Mn^{IV} centers accurately describes the observed ^{55}Mn hyperfine interactions. In the trimer-monomer model, three Mn^{IV} (S = 3/2) centers couple ferromagnetically, giving an S = 9/2 fragment. This fragment then couples antiferromagnetically with the fourth Mn^{IV} center to give an overall S = 3 spin ground state. Importantly, computational studies on the S_3^B model of the S_3 state with a trimer-monomer magnetic coupling scheme produces spin projection factors that estimate the observed A to be on the order of |70−90| MHz, with a unique A holding an opposite sign to the rest. This model is in good agreement with our EDNMR results (Table 1). Additionally, scaling the observed hyperfine coupling interactions in the

ferromagnetically coupled $S = 9/2$ $CaMn_3^{IV}O_4$ complex using the spin projection factors for the trimer-monomer model yield ^{55}Mn hyperfine interactions that are in excellent agreement with the values obtained for **3**. Altogether, the EDNMR data of **3** is consistent with the trimer-monomer magnetic coupling model of pseudo-octahedral Mn^{IV} centers in which the ferromagnetically coupled subunit comprised of Mn2, Mn3, and Mn4 couples antiferromagnetically to Mn1 to give an overall $S = 3$ spin ground state.

DISCUSSION

In the Kok cycle, each S_n state adopts a characteristic spin ground state that is intimately connected to the Mn oxidation states and the overall structure of the Mn-oxo core.[74] Within the ensemble of the various S_n states present in PSII samples, such differences in spin state provide unique, differentiating spectroscopic features that can be exploited in EPR studies of the OEC. In the case of the S_3 state, an effective $S = 3$ spin ground state gives rise to a broad EPR signal that distinguishes the S_3 state from the S_2 state, which features a narrower EPR signal rising from an $S = 1/2$ ground state.[5] The higher $S = 3$ spin state of the S_3 state is notable, as the OEC adopts low spin state electronic structures in the earlier S_0 ($S = 1/2$) and S_1 ($S = 0$) states.[75–76] In the S_3 state, the small anisotropy of the ^{55}Mn hyperfine interactions has been interpreted as rising from the presence of all-octahedral Mn^{IV} centers. The relative sign and magnitude of the ^{55}Mn hyperfine interactions inform about the magnetic exchange coupling interactions between the Mn^{IV} centers. In turn, magnetic coupling interactions are highly sensitive to the structure of the complex, and two limiting models S_3^A and S_3^B have been considered computationally, with S_3^A better accommodating the experimental data.[5] Recently, an altered form of the S_3 state was generated via treatment with methanol.[63] This chemically modified S_3^{MeOH} state exhibits a larger ZFS than that of untreated form ($|D| = 0.281$ vs $0.175\ cm^{-1}$) by virtue of a five-coordinate Mn^{IV} at the dangler Mn site. This form of the S_3 state with a larger ZFS is also observed in the untreated S_3 state, but in a lower concentration. Importantly, the isotropic ^{55}Mn hyperfine interactions in S_3^{MeOH} are consistent with the trimer-monomer magnetic coupling model similar to the S_3^B form (Figure 1a). Reported ^{55}Mn hyperfine interactions of S_3^{MeOH} are on the order of $|60-100|$ MHz, in close agreement with our experimental values (Table 1).[63]

Oxidation of the previously reported $Mn^{III}Mn_3^{IV}O_4$ (**2**) complex featuring an $S = 1/2$ ground state[24] leads to a $Mn^{IV}{}_4O_4$ (**3**) complex with an $S = 3$ ground state, modeling the spin state change behavior of the $S_2 \rightarrow S_3$ transition in the OEC. The structure of **3** and its $Mn^{IV}{}_4$ oxidation state assignment is supported by the rising edge energy of the XANES spectrum and the similar EXAFS spectrum between **2** and **3**. EPR spectra at both X- and D-band frequencies support the $S = 3$ spin state assignment. Most importantly, observed ^{55}Mn hyperfine interactions (A) support a magnetic coupling model proposed for the trimer-monomer model for S_3^B and and S_3^{MeOH}, in which a ferromagnetically coupled trimetallic $S = 9/2$ subunit is coupled antiferromagnetically to the fourth Mn center to yield an $S = 3$ effective spin ground state. The intrinsic, on-site ^{55}Mn hyperfine interaction (a), which is a function of the oxidation state of the Mn center and its coordination geometry, is scaled according to a spin projection factor (ρ) that reflects the nature of the magnetic exchange coupling within the cluster. In addition to the reported $a \approx 180$ MHz for a ferromagnetically coupled $S = 9/2$ $CaMn_3^{IV}O_4$ complex, on-site Mn^{IV} hyperfine values of $a \approx 200$ MHz have

been reported for mononuclear and dinuclear Mn^{IV} complexes.[71, 77–79] As shown in Table 1, the observed A for **3** is in good agreement with the value obtained by scaling the on-site Mn^{IV} hyperfine interaction by the spin projection factor of the trimer-monomer model. Similar to the spin projection factor ρ, a second coefficient κ_i is needed to scale the site fine structure d_i to the measured zero field splitting D, according to the expression $D = \Sigma\kappa_i d_i$.[5, 63] Assuming a site value of $d_i \approx 1\ cm^{-1}$ for two sites, with the remainder being $d_i \approx 0.3\ cm^{-1}$, a total D of 0.4 cm^{-1} can be achieved using the κ_i for the trimer-monomer model[63]: D = (0.15)(1 cm^{-1}) + (0.15)(1 cm^{-1}) + (0.15)(0.3 cm^{-1}) + (0.08)(0.3 cm^{-1}) = 0.37 cm^{-1}. This rough analysis illustrates the point that the measured D of 0.4 cm^{-1} likely arises from multiple distorted octahedral sites in **3**, as further evident from the relatively larger estimated hyperfine anisotropy of **3**.

In conclusion, a unique $Mn^{IV}_4O_4$ cuboidal complex has been synthesized and characterized by XAS, CW-EPR, and pulsed-EPR spectroscopies. To our knowledge this is the first set of experimental studies that directly probes the electronic structure of a tetranuclear Mn^{IV}_4 complex with an $S = 3$ spin ground state mimicking the S_3 state of the OEC. Our studies provide a synthetic precedent for the $S = 1/2 \rightarrow 3$ spin state change that is characteristic of the $S_2 \rightarrow S_3$ transition in the OEC. The magnetic coupling scheme in the $Mn^{IV}_4O_4$ cuboidal complex resemble that of a recently characterized form of the S_3 state of the OEC.[63]

Supplementary Material

Refer to Web version on PubMed Central for supplementary material.

ACKNOWLEDGMENT

D.A.M. thanks Prof. Troy Stich (Wake Forest University) for valuable discussions and for reading the paper. This research was supported by the NIH (R01-GM102687B), the Dreyfus Teacher-Scholar Program (T.A.), Dow Next Generation Educator (instrumentation), NSF-1531940 (Caltech EPR facility), the Division of Chemical Sciences, Geosciences, and Biosciences (R.D.B. grant DE-SC0007203) of the Office of Basic Energy Sciences of the U.S. Department of Energy. Part of this work (XAS data collection) was carried out at Stanford Synchrotron Radiation Lightsource, SLAC National Accelerator Laboratory, supported by the U.S. Department of Energy, Office of Science, Office of Basic Energy Sciences under Contract No. DE-AC02-76SF00515. XAS studies were performed with support of the Office of Science, OBES, Division of Chemical Sciences, Geosciences, and Biosciences (CSGB) of the DOE under contract no. DE-AC02-05CH11231 (J.Y.).

REFERENCES

(1). Pantazis DA, Missing Pieces in the Puzzle of Biological Water Oxidation. ACS Catal. 2018, 8, 9477.

(2). Shen J-R, The Structure of Photosystem II and the Mechanism of Water Oxidation in Photosynthesis. Annu. Rev. Plant Biol 2015, 66, 23. [PubMed: 25746448]

(3). Yano J; Yachandra V, Mn_4Ca Cluster in Photosynthesis: Where and How Water is Oxidized to Dioxygen. Chem. Rev 2014, 114, 4175. [PubMed: 24684576]

(4). Cox N; Pantazis DA; Neese F; Lubitz W, Biological Water Oxidation. Acc. Chem. Res 2013, 46, 1588. [PubMed: 23506074]

(5). Cox N; Retegan M; Neese F; Pantazis DA; Boussac A; Lubitz W, Electronic structure of the oxygen-evolving complex in photosystem II prior to O-O bond formation. Science 2014, 345, 804. [PubMed: 25124437]

(6). Boussac A; Sugiura M; Rutherford AW; Dorlet P, Complete EPR Spectrum of the S_3-State of the Oxygen-Evolving Photosystem II. J. Am. Chem. Soc 2009, 131, 5050. [PubMed: 19320479]

(7). DeRose VJ; Latimer MJ; Zimmermann J-L; Mukerji I; Yachandra VK; Sauer K; Klein MP, Fluoride substitution in the Mn cluster from Photosystem II: EPR and X-ray absorption spectroscopy studies. Chem. Phys 1995, 194, 443.

(8). Oyala PH; Stich TA; Debus RJ; Britt RD, Ammonia Binds to the Dangler Manganese of the Photosystem II Oxygen-Evolving Complex. J. Am. Chem. Soc 2015, 137, 8829. [PubMed: 26083545]

(9). Beal NJ; Corry TA; O'Malley PJ, A Comparison of Experimental and Broken Symmetry Density Functional Theory (BS-DFT) Calculated Electron Paramagnetic Resonance (EPR) Parameters for Intermediates Involved in the S_2 to S_3 State Transition of Nature's Oxygen Evolving Complex. J. Phys. Chem. B 2018, 122, 1394. [PubMed: 29300480]

(10). Kern J; Chatterjee R; Young ID; Fuller FD; Lassalle L; Ibrahim M; Gul S; Fransson T; Brewster AS; Alonso-Mori R; Hussein R; Zhang M; Douthit L; de Lichtenberg C; Cheah MH; Shevela D; Wersig J; Seuffert I; Sokaras D; Pastor E; Weninger C; Kroll T; Sierra RG; Aller P; Butryn A; Orville AM; Liang M; Batyuk A; Koglin JE; Carbajo S; Boutet S; Moriarty NW; Holton JM; Dobbek H; Adams PD; Bergmann U; Sauter NK; Zouni A; Messinger J; Yano J; Yachandra VK, Structures of the intermediates of Kok's photosynthetic water oxidation clock. Nature 2018, 563, 421. [PubMed: 30405241]

(11). Isobe H; Shoji M; Shen J-R; Yamaguchi K, Chemical Equilibrium Models for the S_3 State of the Oxygen-Evolving Complex of Photosystem II. Inorg. Chem 2016, 55, 502. [PubMed: 26717045]

(12). Askerka M; Wang J; Vinyard DJ; Brudvig GW; Batista VS, S_3 State of the O_2-Evolving Complex of Photosystem II: Insights from QM/MM, EXAFS, and Femtosecond X-ray Diffraction. Biochemistry 2016, 55, 981. [PubMed: 26849148]

(13). Retegan M; Krewald V; Mamedov F; Neese F; Lubitz W; Cox N; Pantazis DA, A five-coordinate Mn(iv) intermediate in biological water oxidation: spectroscopic signature and a pivot mechanism for water binding. Chem. Sci 2016, 7, 72. [PubMed: 29861966]

(14). Weng T-C; Hsieh W-Y; Uffelman ES; Gordon-Wylie SW; Collins TJ; Pecoraro VL; Penner-Hahn JE, XANES Evidence Against a Manganyl Species in the S_3 State of the Oxygen-Evolving Complex. J. Am. Chem. Soc 2004, 126, 8070. [PubMed: 15225020]

(15). Ioannidis N; Nugent JHA; Petrouleas V, Intermediates of the S_3 State of the Oxygen-Evolving Complex of Photosystem II. Biochemistry 2002, 41, 9589. [PubMed: 12135381]

(16). Geijer P; Morvaridi F; Styring S, The S_3 State of the Oxygen-Evolving Complex in Photosystem II Is Converted to the $S_2Y_Z^{\bullet}$ State at Alkaline pH. Biochemistry 2001, 40, 10881. [PubMed: 11535065]

(17). Ioannidis N; Petrouleas V, Electron Paramagnetic Resonance Signals from the S3 State of the Oxygen-Evolving Complex. A Broadened Radical Signal Induced by Low-Temperature Near-Infrared Light Illumination. Biochemistry 2000, 39, 5246. [PubMed: 10819993]

(18). Liang W; Roelofs TA; Cinco RM; Rompel A; Latimer MJ; Yu WO; Sauer K; Klein MP; Yachandra VK, Structural Change of the Mn Cluster during the $S_2 \rightarrow S_3$ State Transition of the Oxygen-Evolving Complex of Photosystem II. Does It Reflect the Onset of Water/Substrate Oxidation? Determination by Mn X-ray Absorption Spectroscopy. J. Am. Chem. Soc 2000, 122, 3399. [PubMed: 25152534]

(19). Matsukawa T; Mino H; Yoneda D; Kawamori A, Dual-Mode EPR Study of New Signals from the S_3-State of Oxygen-Evolving Complex in Photosystem II. Biochemistry 1999, 38, 4072. [PubMed: 10194321]

(20). Wincencjusz H; van Gorkom HJ; Yocum CF, The Photosynthetic Oxygen Evolving Complex Requires Chloride for Its Redox State $S_2 \rightarrow S_3$ and $S_3 \rightarrow S_0$ Transitions But Not for $S_0 \rightarrow S_1$ or $S_1 \rightarrow S_2$ Transitions. Biochemistry 1997, 36, 3663. [PubMed: 9132019]

(21). Messinger J; Badger M; Wydrzynski T, Detection of one slowly exchanging substrate water molecule in the S_3 state of photosystem II. Proc. Nat. Acad. Sci 1995, 92, 3209. [PubMed: 11607525]

(22). MacLachlan DJ; Nugent JHA; Evans MCW, A XANES study of the manganese complex of inhibited PS II membranes indicates manganese redox changes between the modified S_1, S_2 and S_3 states. Biochim. et Biophys. Acta - Bioenergetics 1994, 1185, 103.

(23). Boussac A; Zimmermann JL; Rutherford AW, EPR signals from modified charge accumulation states of the oxygen-evolving enzyme in calcium-deficient photosystem II. Biochemistry 1989, 28, 8984. [PubMed: 2557913]

(24). Lee HB; Shiau AA; Oyala PH; Marchiori DA; Gul S; Chatterjee R; Yano J; Britt RD; Agapie T, Tetranuclear [$Mn^{III}Mn3IVO_4$] Complexes as Spectroscopic Models of the S_2 State of the Oxygen Evolving Complex in Photosystem II. J. Am. Chem. Soc 2018, 140, 17175. [PubMed: 30407806]

(25). Reed CJ; Agapie T, Thermodynamics of Proton and Electron Transfer in Tetranuclear Clusters with Mn–OH_2/OH Motifs Relevant to H_2O Activation by the Oxygen Evolving Complex in Photosystem II. J. Am. Chem. Soc 2018, 140, 10900. [PubMed: 30064207]

(26). Paul S; Neese F; Pantazis DA, Structural models of the biological oxygen-evolving complex: achievements, insights, and challenges for biomimicry. Green Chem. 2017, 19, 2309.

(27). Han Z; Horak KT; Lee HB; Agapie T, Tetranuclear Manganese Models of the OEC Displaying Hydrogen Bonding Interactions: Application to Electrocatalytic Water Oxidation to Hydrogen Peroxide. J. Am. Chem. Soc 2017, 139, 9108. [PubMed: 28587453]

(28). Lee HB; Tsui EY; Agapie T, A $CaMn_4O_2$ model of the biological oxygen evolving complex: synthesis via cluster expansion on a low symmetry ligand. Chem. Commun 2017, 53, 6832.

(29). Zhang C; Chen C; Dong H; Shen J-R; Dau H; Zhao J, A synthetic Mn_4Ca-cluster mimicking the oxygen-evolving center of photosynthesis. Science 2015, 348, 690. [PubMed: 25954008]

(30). Kanady JS; Lin P-H; Carsch KM; Nielsen RJ; Takase MK; Goddard WA; Agapie T, Toward Models for the Full Oxygen-Evolving Complex of Photosystem II by Ligand Coordination To Lower the Symmetry of the Mn_3CaO_4 Cubane: Demonstration That Electronic Effects Facilitate Binding of a Fifth Metal. J. Am. Chem. Soc 2014, 136, 14373. [PubMed: 25241826]

(31). Kanady JS; Mendoza-Cortes JL; Tsui EY; Nielsen RJ; Goddard WA; Agapie T, Oxygen Atom Transfer and Oxidative Water Incorporation in Cuboidal Mn_3MO_n Complexes Based on Synthetic, Isotopic Labeling, and Computational Studies. J. Am. Chem. Soc 2013, 135, 1073. [PubMed: 23241061]

(32). Kanady JS; Tran R; Stull JA; Lu L; Stich TA; Day MW; Yano J; Britt RD; Agapie T, Role of oxido incorporation and ligand lability in expanding redox accessibility of structurally related Mn_4 clusters. Chem. Sci 2013, 4, 3986. [PubMed: 24163730]

(33). Tsui EY; Agapie T, Reduction potentials of heterometallic manganese–oxido cubane complexes modulated by redox-inactive metals. Proc. Nat. Acad. Sci 2013, 110, 10084. [PubMed: 23744039]

(34). Tsui EY; Kanady JS; Agapie T, Synthetic Cluster Models of Biological and Heterogeneous Manganese Catalysts for O_2 Evolution. Inorg. Chem 2013, 52, 13833. [PubMed: 24328344]

(35). Tsui EY; Tran R; Yano J; Agapie T, Redox-inactive metals modulate the reduction potential in heterometallic manganese–oxido clusters. Nat. Chem 2013, 5, 293. [PubMed: 23511417]

(36). Mukherjee S; Stull JA; Yano J; Stamatatos TC; Pringouri K; Stich TA; Abboud KA; Britt RD; Yachandra VK; Christou G, Synthetic model of the asymmetric [Mn_3CaO_4] cubane core of the oxygen-evolving complex of photosystem II. Proc. Nat. Acad. Sci 2012, 109, 2257. [PubMed: 22308383]

(37). Kanady JS; Tsui EY; Day MW; Agapie T, A Synthetic Model of the Mn_3Ca Subsite of the Oxygen-Evolving Complex in Photosystem II. Science 2011, 333, 733. [PubMed: 21817047]

(38). Mukhopadhyay S; Mandal SK; Bhaduri S; Armstrong WH, Manganese Clusters with Relevance to Photosystem II. Chem. Rev 2004, 104, 3981. [PubMed: 15352784]

(39). Morton J; Chrysina M; Craig VSJ; Akita F; Nakajima Y; Lubitz W; Cox N; Shen J-R; Krausz E, Structured near-infrared Magnetic Circular Dichroism spectra of the Mn_4CaO_5 cluster of PSII in T. vulcanus are dominated by Mn(IV) d-d 'spin-flip' transitions. Biochim. et Biophys. Acta - Bioenergetics 2018, 1859, 88.

(40). Schuth N; Zaharieva I; Chernev P; Berggren G; Anderlund M; Styring S; Dau H; Haumann M, Kα X-ray Emission Spectroscopy on the Photosynthetic Oxygen-Evolving Complex Supports Manganese Oxidation and Water Binding in the S_3 State. Inorg. Chem 2018, 57, 10424. [PubMed: 30067343]

(41). Krewald V; Retegan M; Cox N; Messinger J; Lubitz W; DeBeer S; Neese F; Pantazis DA, Metal oxidation states in biological water splitting. Chem. Sci 2015, 6, 1676. [PubMed: 29308133]

(42). Boussac A; Rutherford AW; Sugiura M, Electron transfer pathways from the S_2-states to the S_3-states either after a Ca^{2+}/Sr^{2+} or a Cl^{-}/I^{-} exchange in Photosystem II from Thermosynechococcus elongatus. Biochim. et Biophys. Acta - Bioenergetics 2015, 1847, 576.

(43). Pantazis DA; Ames W; Cox N; Lubitz W; Neese F, Two Interconvertible Structures that Explain the Spectroscopic Properties of the Oxygen-Evolving Complex of Photosystem II in the S_2 State. Angew. Chem. Int. Ed 2012, 51, 9935.

(44). Isobe H; Shoji M; Yamanaka S; Mino H; Umena Y; Kawakami K; Kamiya N; Shen JR; Yamaguchi K, Generalized approximate spin projection calculations of effective exchange integrals of the $CaMn_4O_5$ cluster in the S_1 and S_3 states of the oxygen evolving complex of photosystem II. Phys. Chem. Chem. Phys 2014, 16, 11911. [PubMed: 24632787]

(45). Suga M; Akita F; Sugahara M; Kubo M; Nakajima Y; Nakane T; Yamashita K; Umena Y; Nakabayashi M; Yamane T; Nakano T; Suzuki M; Masuda T; Inoue S; Kimura T; Nomura T; Yonekura S; Yu L-J; Sakamoto T; Motomura T; Chen J-H; Kato Y; Noguchi T; Tono K; Joti Y; Kameshima T; Hatsui T; Nango E; Tanaka R; Naitow H; Matsuura Y; Yamashita A; Yamamoto M; Nureki O; Yabashi M; Ishikawa T; Iwata S; Shen J-R, Light-induced structural changes and the site of O=O bond formation in PSII caught by XFEL. Nature 2017, 543, 131. [PubMed: 28219079]

(46). Chen; Collomb M-N; Duboc C; Blondin G; Rivière E; Faller JW; Crabtree RH; Brudvig GW, New Linear High-Valent Tetranuclear Manganese-Oxo Cluster Relevant to the Oxygen-Evolving Complex of Photosystem II with Oxo, Hydroxo, and Aqua Coordinated to a Single Mn(IV). Inorg. Chem 2005, 44, 9567. [PubMed: 16323946]

(47). Dubé CE; Mukhopadhyay S; Bonitatebus PJ; Staples RJ; Armstrong WH, Tuning Tetranuclear Manganese–Oxo Core Electronic Properties: Adamantane-Shaped Complexes Synthesized by Ligand Exchange. Inorg. Chem 2005, 44, 5161. [PubMed: 15998046]

(48). Chen H; Faller JW; Crabtree RH; Brudvig GW, Dimer-of-Dimers Model for the Oxygen-Evolving Complex of Photosystem II. Synthesis and Properties of $[Mn^{IV}4O_5(terpy)_4(H_2O)_2](ClO_4)_6$. J. Am. Chem. Soc 2004, 126, 7345. [PubMed: 15186173]

(49). Mukhopadhyay S; Staples RJ; Armstrong WH, Toward synthetic models for high oxidation state forms of the Photosystem II active site metal cluster: the first tetranuclear manganese cluster containing a $[Mn_4(\mu\text{-}O)_5]^{6+}$ core. Chem. Commun 2002, 864.

(50). Dubé CE; Wright DW; Pal S; Bonitatebus PJ; Armstrong WH, Tetranuclear Manganese-Oxo Aggregates Relevant to the Photosynthetic Water Oxidation Center. Crystal Structure, Spectroscopic Properties and Reactivity of Adamantane-Shaped $[Mn_4O_6(bpea)_4]^{4+}$ and the Reduced Mixed-Valence Analog $[Mn_4O_6(bpea)_4]^{3+}$. J. Am. Chem. Soc 1998, 120, 3704.

(51). Philouze C; Blondin G; Girerd J-J; Guilhem J; Pascard C; Lexa D, Aqueous Chemistry of High-Valent Manganese. Structure, Magnetic, and Redox Properties of a New Type of Mn-Oxo Cluster, $[Mn4IVO_4(bpy)_6]^{4+}$: Relevance to the Oxygen Evolving Center in Plants. J. Am. Chem. Soc 1994, 116, 8557.

(52). Hagen KS; Westmoreland TD; Scott MJ; Armstrong WH, Structural and electronic consequences of protonation in $\{Mn_4O_6\}^{4+}$ cores: pH dependent properties of oxo-bridged manganese complexes. J. Am. Chem. Soc 1989, 111, 1907.

(53). Blondin G; Davydov R; Philouze C; Charlot M-F; Styring S; Akermark B; Girerd J-J; Boussac A, Electron paramagnetic resonance study of the S=1/2 ground state of a radiolysis-generated manganese(III)-trimanganese(IV) form of $[Mn^{IV}4O_6(bipy)_6]^{4+}$ (bipy=2,2'-bipyridine). Comparison with the photosynthetic Oxygen Evolving Complex. J. Chem. Soc. Dalton Trans 1997, 4069.

(54). Dubé CE; Sessoli R; Hendrich MP; Gatteschi D; Armstrong WH, A Spin Topological Model for the g = 4.1 S_2 State Photosystem II Water Oxidase Manganese Aggregate. J. Am. Chem. Soc 1999, 121, 3537.

(55). Gupta R; Taguchi T; Lassalle-Kaiser B; Bominaar EL; Yano J; Hendrich MP; Borovik AS, High-spin Mn–oxo complexes and their relevance to the oxygen-evolving complex within photosystem II. Proc. Nat. Acad. Sci 2015, 112, 5319. [PubMed: 25852147]

(56). Steckhan E, Indirect Electroorganic Syntheses—A Modern Chapter of Organic Electrochemistry [New Synthetic Methods (59)]. Angew. Chem. Int. Ed 1986, 25, 683.

(57). Yueh W; Bauld NL, Mechanistic Criteria for Cation Radical Reactions: Aminium Salt-Catalyzed Cyclopropanation. J. Am. Chem. Soc 1995, 117, 5671.

(58). Glöckner C; Kern J; Broser M; Zouni A; Yachandra V; Yano J, Structural Changes of the Oxygen-evolving Complex in Photosystem II during the Catalytic Cycle. J. Biol. Chem 2013, 288, 22607. [PubMed: 23766513]

(59). Sturgeon BE; Ball JA; Randall DW; Britt RD, ^{55}Mn Electron Spin Echo ENDOR of Mn^{2+} Complexes. J. Phys. Chem 1994, 98, 12871.

(60). Stich T; Lahiri S; Yeagle G; Dicus M; Brynda M; Gunn A; Aznar C; DeRose V; Britt R, Multifrequency pulsed EPR studies of biologically relevant manganese (II) complexes. Appl. Mag. Reson 2007, 31, 321.

(61). Tomioka H; Hattori M; Hirai K; Sato K; Shiomi D; Takui T; Itoh K, Persistent High-Spin Polycarbene. Generation of Polybrominated 1,3,5-Tris-[2-[4-(Phenylcarbeno)-phenyl]ethynyl]benzene (S = 3) and Spin Identification by Two-Dimensional Electron Spin Transient Nutation Spectroscopy. J. Am. Chem. Soc 1998, 120, 1106.

(62). Juarez-Garcia C; Hendrich MP; Holman TR; Que L; Munck E, Combined Moessbauer and EPR studies of the $S = 3$ state of an exchange-coupled iron(III)-copper(II) complex: test for quantitative EPR analysis of integer spin systems. J. Am. Chem. Soc 1991, 113, 518.

(63). Chrysina M; Heyno E; Kutin Y; Reus M; Nilsson H; Nowaczyk MM; DeBeer S; Neese F; Messinger J; Lubitz W; Cox N, Five-coordinate Mn^{IV} intermediate in the activation of nature's water splitting cofactor. Proc. Nat. Acad. Sci 2019, 116, 16841. [PubMed: 31391299]

(64). Cox N; Rapatskiy L; Su J-H; Pantazis DA; Sugiura M; Kulik L; Dorlet P; Rutherford AW; Neese F; Boussac A; Lubitz W; Messinger J, Effect of Ca^{2+}/Sr^{2+} Substitution on the Electronic Structure of the Oxygen-Evolving Complex of Photosystem II: A Combined Multifrequency EPR, ^{55}Mn-ENDOR, and DFT Study of the S_2 State. J. Am. Chem. Soc 2011, 133, 3635. [PubMed: 21341708]

(65). Duboc C; Collomb M-N, Multifrequency high-field EPR investigation of a mononuclear manganese(iv) complex. Chem. Commun 2009, 2715.

(66). Dolai M; Amjad A; Debnath M; Tol J. v.; Barco E. d.; Ali M, Water-Stable Manganese(IV) Complex of a N_2O_4-Donor Non-Schiff-Base Ligand: Synthesis, Structure, and Multifrequency High-Field Electron Paramagnetic Resonance Studies. Inorg. Chem 2014, 53, 5423. [PubMed: 24824101]

(67). Leto DF; Massie AA; Colmer HE; Jackson TA, X-Band Electron Paramagnetic Resonance Comparison of Mononuclear Mn^{IV}-oxo and Mn^{IV}-hydroxo Complexes and Quantum Chemical Investigation of Mn^{IV} Zero-Field Splitting. Inorg. Chem 2016, 55, 3272. [PubMed: 27002928]

(68). Zlatar M; Gruden M; Vassilyeva OY; Buvaylo EA; Ponomarev AN; Zvyagin SA; Wosnitza J; Krzystek J; Garcia-Fernandez P; Duboc C, Origin of the Zero-Field Splitting in Mononuclear Octahedral Mn^{IV} Complexes: A Combined Experimental and Theoretical Investigation. Inorg. Chem 2016, 55, 1192. [PubMed: 26745448]

(69). Cox N; Lubitz W; Savitsky A, W-band ELDOR-detected NMR (EDNMR) spectroscopy as a versatile technique for the characterisation of transition metal-ligand interactions. Mol. Phys 2013, 111, 2788.

(70). Schosseler P; Wacker T; Schweiger A, Pulsed ELDOR detected NMR. Chem. Phys. Lett 1994, 224, 319.

(71). Nguyen AI; Suess DLM; Darago LE; Oyala PH; Levine DS; Ziegler MS; Britt RD; Tilley TD, Manganese-Cobalt Oxido Cubanes Relevant to Manganese-Doped Water Oxidation Catalysts. J. Am. Chem. Soc 2017, 139, 5579. [PubMed: 28347135]

(72). Andresen HG, Electron Paramagnetic Resonance of Manganese in TiO_2. Phys. Rev 1960, 120, 1606.

(73). From WH; Dorain PB; Kikuchi C, Hyperfine and Superhyperfine Structure of Manganese in SnO_2. Phys. Rev 1964, 135, A710.

(74). Krewald V; Retegan M; Neese F; Lubitz W; Pantazis DA; Cox N, Spin State as a Marker for the Structural Evolution of Nature's Water-Splitting Catalyst. Inorg. Chem 2016, 55, 488. [PubMed: 26700960]

(75). Kulik LV; Epel B; Lubitz W; Messinger J, Electronic Structure of the Mn_4O_xCa Cluster in the S_0 and S_2 States of the Oxygen-Evolving Complex of Photosystem II Based on Pulse ^{55}Mn-ENDOR and EPR Spectroscopy. J. Am. Chem. Soc 2007, 129, 13421. [PubMed: 17927172]

(76). Yamauchi T; Mino H; Matsukawa T; Kawamori A; Ono T. a., Parallel Polarization Electron Paramagnetic Resonance Studies of the S_1-State Manganese Cluster in the Photosynthetic Oxygen-Evolving System. Biochemistry 1997, 36, 7520. [PubMed: 9200702]

(77). Parsell TH; Behan RK; Green MT; Hendrich MP; Borovik AS, Preparation and Properties of a Monomeric Mn^{IV}−Oxo Complex. J. Am. Chem. Soc 2006, 128, 8728. [PubMed: 16819856]

(78). Randall DW; Sturgeon BE; Ball JA; Lorigan GA; Chan MK; Klein MP; Armstrong WH; Britt RD, ^{55}Mn ESE-ENDOR of a Mixed Valence Mn(III)Mn(IV) Complex: Comparison with the Mn Cluster of the Photosynthetic Oxygen-Evolving Complex. J. Am. Chem. Soc 1995, 117, 11780.

(79). Schäfer K-O; Bittl R; Zweygart W; Lendzian F; Haselhorst G; Weyhermüller T; Wieghardt K; Lubitz W, Electronic Structure of Antiferromagnetically Coupled Dinuclear Manganese ($Mn^{III}Mn^{IV}$) Complexes Studied by Magnetic Resonance Techniques. J. Am. Chem. Soc 1998, 120, 13104.

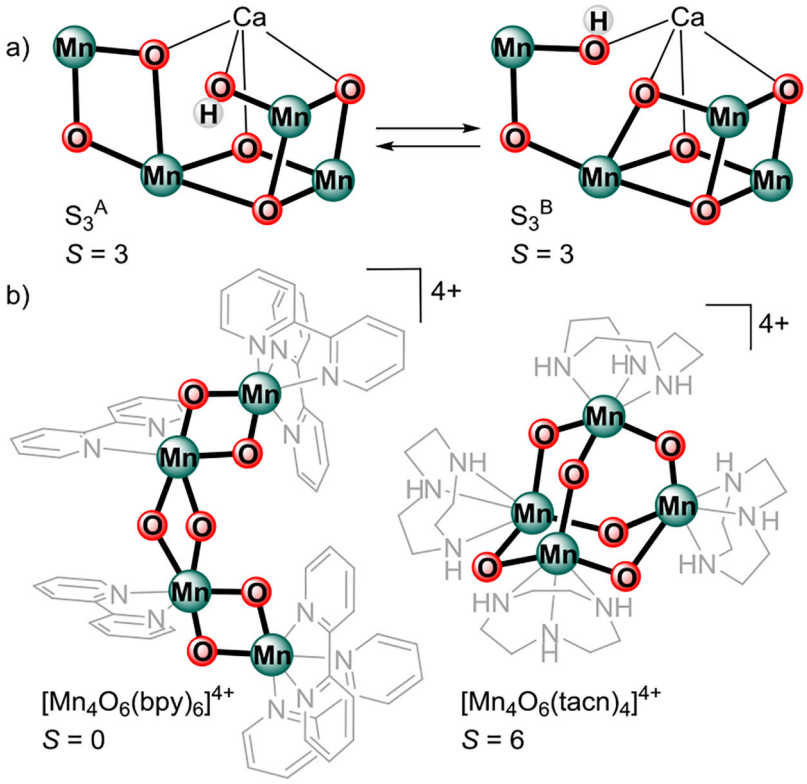

Figure 1.

a) Proposed isomers S_3^A and S_3^B of the inorganic $CaMn_4O_5(OH)$ core of the S_3 state of the OEC. b) Representative examples of Mn^{IV}_4 complexes and their corresponding spin ground states.

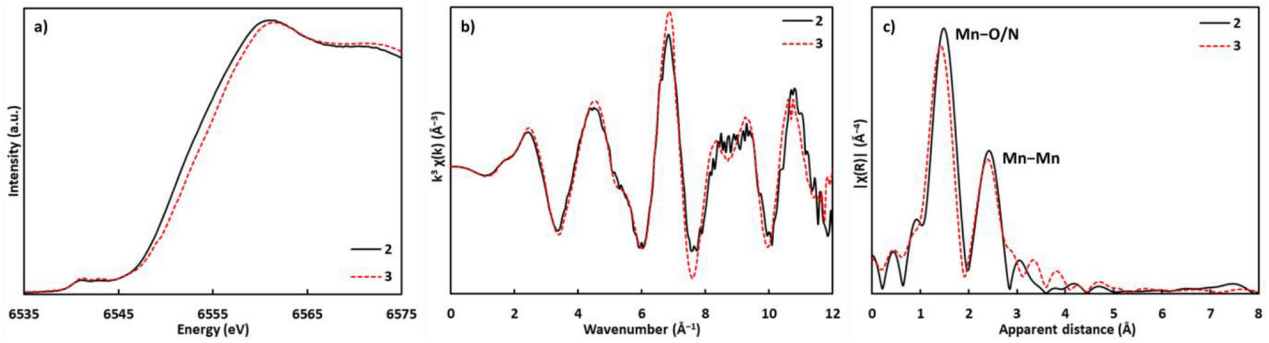

Figure 2.

Mn *K*-edge XAS spectra for complexes **2** (black lines) and **3** (red dotted lines). a) Normalized XANES data, b) k^3-weighted EXAFS data, and c) Fourier transforms of k^3-weighted EXAFS data.

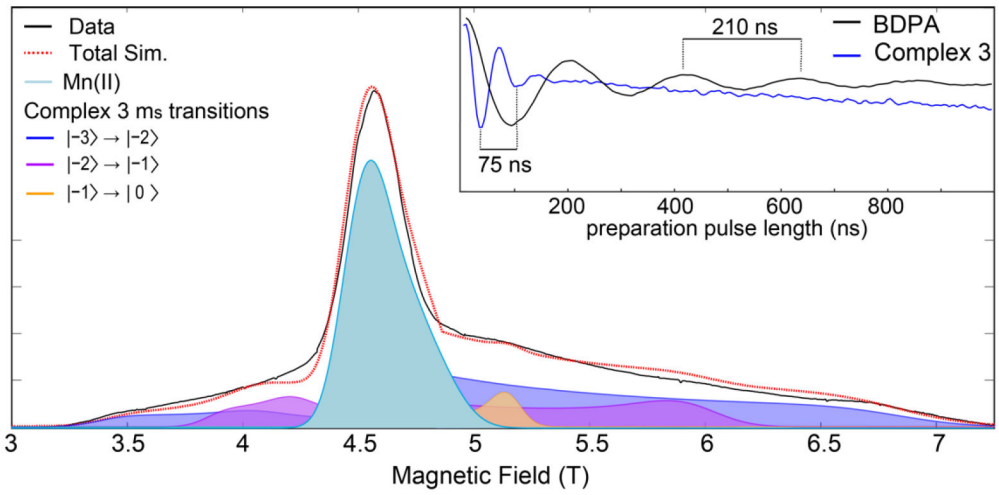

Figure 3.

D-band EPR spectrum of complex **3** collected at 1.6 K. Spectral data are shown in black and the simulated spectrum is represented by the dashed red line and other colored traces. The simulated Mn(II) contribution is shown in light blue and the m_S transitions that contribute to the complex **3** simulation are shown in blue, purple, and orange. Simulation parameters: $S = 3$, $g = 1.97$, $D = 0.4\ cm^{-1}$, $E/D = 0.1$. (Inset) Electron-spin nutation curves of complex **3** (blue) collected at 7 T and BDPA (black).

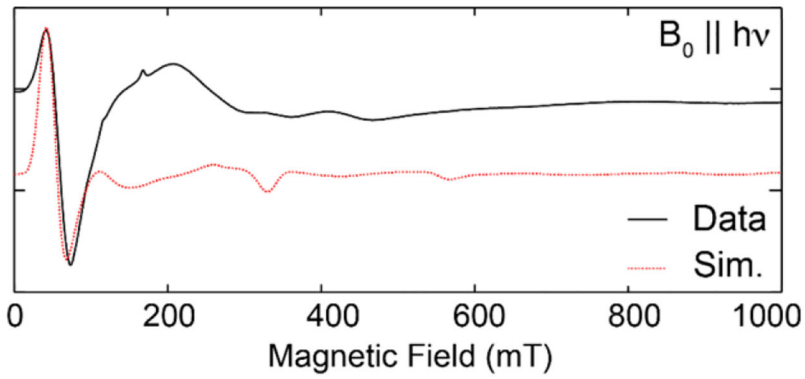

Figure 4.

Parallel mode X-band CW-EPR of complex **3**. Spectral data are shown in black and the simulated spectrum is represented by the dashed red line. Simulation parameters: $S = 3$, $g = 1.97$, $D = 0.4\ cm^{-1}$, $E/D = 0.1$.

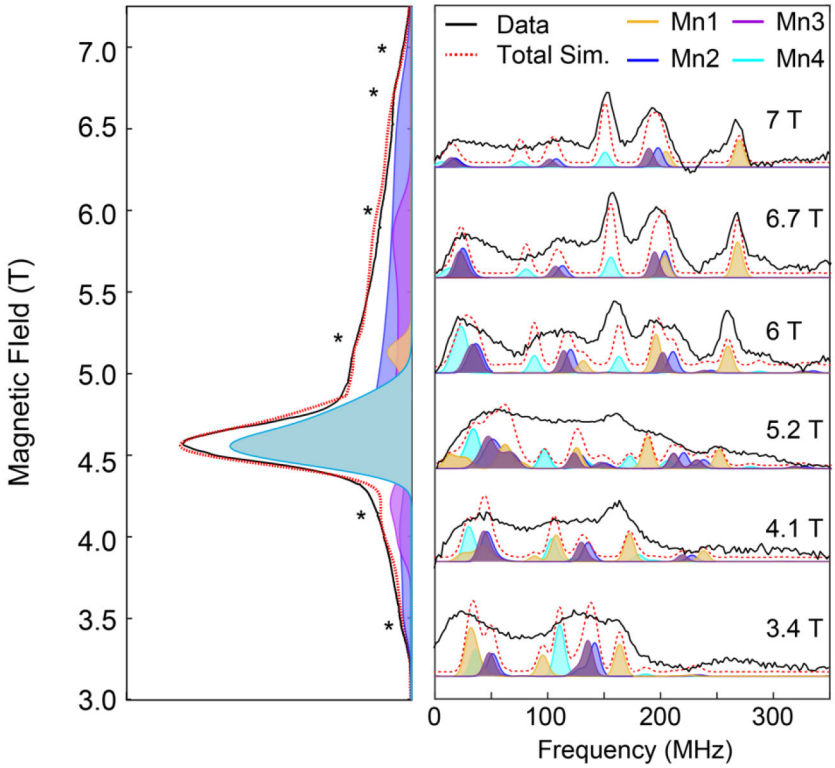

Figure 5.

(Left) EPR spectrum of **3** showing the field positions (*) where EDNMR spectra were collected. (Right) Field dependent EDNMR of **3**. Experimental data are shown in black traces. Spectral simulations are shown in the colored traces. The simulated hyperfine values are listed in Table 1.

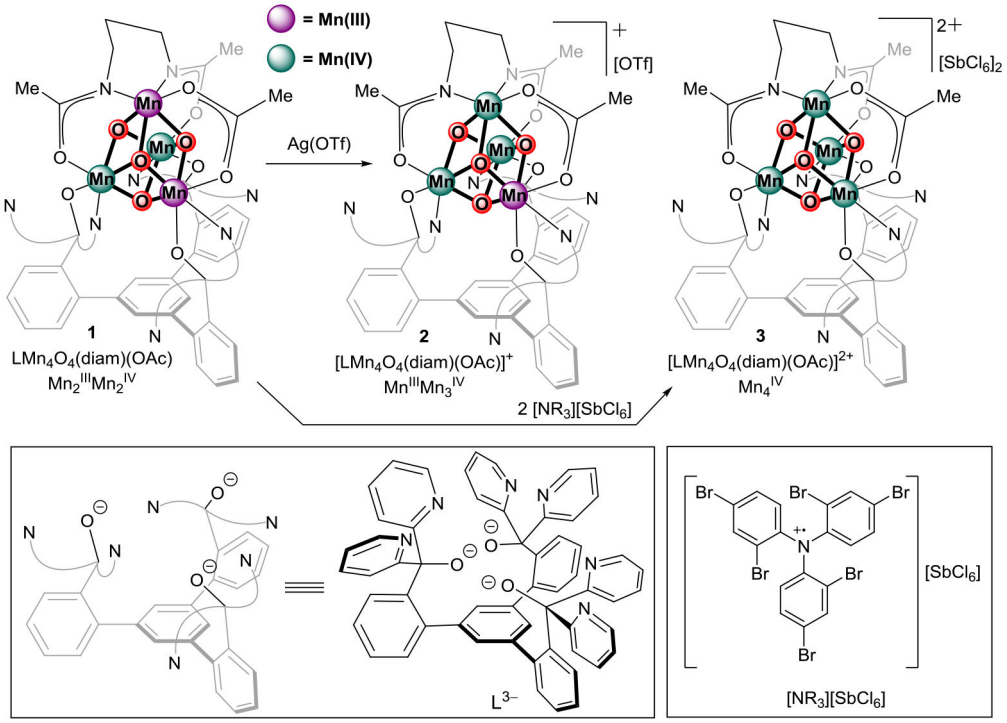

Scheme 1.
Synthesis of complexes **1~3** studied in this work.

Table 1.

Isotropic ^{55}Mn hyperfine interactions (MHz) in complex **3**, different models of the S_3 state[5, 63], and the $CaMn_3^{IV}O_4$ model complex[36].

	Mn1	Mn2	Mn3	Mn4
Projected hyperfine interactions (MHz)				
3	66	−91	−88	−75
S_3^{MeOH} [a]	62	−102	−99	−95
$CaMn_3^{IV}O_4$ model, [b]		−87	−87	−76
S_3^B [c]	86	−75	−79	−65
S_3^A [d]	−99	−96	−26 or 7	≤ 5
On-site hyperfine interactions (MHz)				
3 [e]	−178	−194	−187	−174
S_3^{MeOH} [e]	−166	−222	−216	−207
$CaMn_3^{IV}O_4$ model [f]		−185	−185	−179
S_3^B [g]	−232	−161	−169	−148
Spin projection factors ρ				
Trimer-monomer model [h]	−0.37	0.47	0.47	0.43

[a] Reported ^{55}Mn hyperfine interactions in the MeOH-modified form of the S_3 state.[63]

[b] Projected ^{55}Mn hyperfine interactions for the $CaMn_3^{IV}O_4$ model complex using the trimer-monomer model spin projection factors.[36]

[c] Projected ^{55}Mn hyperfine interactions in the calculated trimer-monomer S_3^B model of the S_3 state.[5]

[d] Reported ^{55}Mn hyperfine interactions for the S_3^A form of the S_3 state.[5]

[e] Estimated on-site ^{55}Mn hyperfine interactions assuming a trimer-monomer model.[63]

[f] Reported ^{55}Mn hyperfine interactions in an $S = 9/2$ $CaMn_3^{IV}O_4$ model complex.[36]

[g] Calculated on-site ^{55}Mn hyperfine interactions in the trimer-monomer S_3^B model of the S_3 state.[5]

[h] Ref 5.